Elucidating Intravoxel Geometry in Diffusion-MRI: Asymmetric Orientation Distribution Functions (AODFs) Revealed by a Cone Model

Suheyla Cetin[1], Evren Ozarslan[2], and Gozde Unal[1]

[1] Faculty of Engineering and Natural Sciences, Sabanci University, Turkey
[2] Physics Department, Bogazici University, Turkey
{suheylacetin,gozdeunal}@sabanciuniv.edu, evren.ozarslan@boun.edu.tr

Abstract. A diffusion-MRI processing method is presented for representing the inherent asymmetry of the underlying intravoxel geometry, which emerges in regions with bending, crossing, or sprouting fibers. The orientation distribution functions (ODFs) obtained through conventional approaches such as q-ball imaging and spherical deconvolution result in symmetric ODF profiles at each voxel even when the underlying geometry is asymmetric. To extract such inherent asymmetry, an inter-voxel filtering approach through a cone model is employed. The cone model facilitates a sharpening of the ODFs in some directions while suppressing peaks in other directions, thus yielding an asymmetric ODF (AODF) field. Compared to symmetric ODFs, AODFs reveal more information regarding the cytoarchitectural organization within the voxel. The level of asymmetry is quantified via a new scalar index that could complement standard measures of diffusion anisotropy. Experiments on synthetic geometries of circular, crossing, and kissing fibers show that the estimated AODFs successfully recover the asymmetry of the underlying geometry. The feasibility of the technique is demonstrated on *in vivo* data obtained from the Human Connectome Project.

Keywords: MRI, diffusion, anisotropy, HARDI, ODF, asymmetry.

1 Introduction

Diffusion magnetic resonance imaging (dMRI) provides a powerful means to characterize tissue anisotropy, enabling the computation of neural connections in the nervous system. Diffusion tensor imaging (DTI) based findings have demonstrated the feasibility of such endeavour [1] despite its well-known shortcoming in regions with heterogeneous fiber orientations. In such environments, the unimodal ODF assumed by DTI is incapable of resolving the orientations of distinct fiber bundles within a voxel.

An important advance is the introduction of high angular resolution diffusion imaging (HARDI) acquisitions [2]. Several methods, designed for HARDI data,

N. Navab et al. (Eds.): MICCAI 2015, Part I, LNCS 9349, pp. 231–238, 2015.
DOI: 10.1007/978-3-319-24553-9_29

have managed to overcome DTI's limitation by making it possible to estimate multimodal ODFs.

Although having multimodal distributions is very important for reliably estimating connectivity, the HARDI-based ODFs do not accurately reflect the underlying cellular organization. For example, it has been demonstrated that when the voxel of interest contains Y-shaped crossings [3], or curving fibers [4], the distribution of displacements for water molecules is asymmetric. Due to the Fourier transform relationship between the displacement distribution and the signal, the signal for such regions is predicted to be complex-valued. Consequently, some techniques [3,5,6] have been formulated with the capability of handling complex-valued data to yield asymmetric profiles.

From a practical point-of-view however, obtaining accurate phase information in diffusion-weighted acquisitions is a formidable task particularly in *in vivo* acquisitions. Most important obstacle is the patient motion, which substantially distorts the phase of the signal [7]. Additionally, imperfections in the acquisition (e.g., imperfect B_0 shift compensation), flow, and susceptibility variations within the tissue could all influence the detected signal phase substantially. Thus, attributing the observed phase shifts to diffusion alone would be very problematic. Therefore, current dMRI processing pipelines assume magnitude-valued data. When magnitude-valued data are used, the regions containing Y-shaped crossings or bending fibers might lead to unimodal or star-shaped ODFs.

Several works have been published with varying levels of relevance to our study. In Ref. [8] the authors suggested an ODF field estimation scheme by considering inter-voxel information, which requires a relatively large number of diffusion directions. The high order tensor method and the associated tensor voting scheme introduced in Ref. [9] was shown to provide even-order tensor fields that facilitate fiber reconstruction at crossings, and odd-order fields that differentiate crossings from junctions. In Ref. [10], tracts with high curvature, crossing, branching, bottlenecks and sprouting have been discussed within the context of partial volume averaging of fiber directions and a regularisation technique was introduced. However, there is no mention of AODFs in this work.

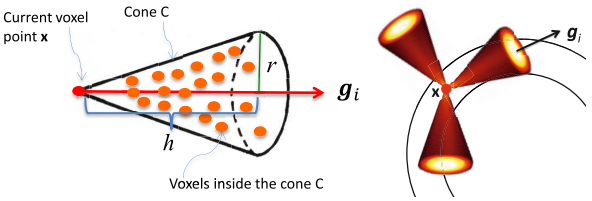

Fig. 1. Left: The cone **C** with a certain height and radius is used in the ODF filtering; Right: An asymmetric ODF is constructed by rotating the cone model along all sampled directions on the unit sphere at each voxel point and performing a weighted averaging using the depicted Gaussian map (shown in hot colours).

In a recent work [11], a regularisation on the ODF field is carried out using a cone model somewhat similar to the one we propose in this work. However, the approach in [11] differs in that ODF regularisation is based on the asymmetric weights assigned to the utilized pair of antipodally-symmetric cones placed at a given voxel. Moreover, neither in the results nor in the discussions is an AODF constructed or depicted.

In this paper, we present a technique for voxel-by-voxel reconstruction of AODFs. To the best of our knowledge this is the first such study.

2 Method

Relying on well-established HARDI techniques[1] that enable estimation of a multi-directional representation of the local fiber orientations, we present a method that exploits voxel-based ODFs in a conic spatial neighborhood to capture underlying asymmetry of the ODF. The ODF is defined at each voxel location $\mathbf{x} = (x, y, z) \in \mathbb{R}^3$ by $\phi_{\mathbf{x}}(\mathbf{g_i})$ for each sampled direction vector $\mathbf{g_i} \in \mathbb{S}^{\mathbf{2}}$. At the given voxel $\mathbf{x}$ and the given direction $\mathbf{g_i}$, a cone $\mathbf{C}$ (Figure 1(a)) is constructed by a certain radius r and height h. Although the directional asymmetry of the fiber pathway cannot be deduced from the ODF of a single voxel, it becomes apparent by considering the information holistically revealed by the ODFs of the voxels in the local volume delimited by the cone $\mathbf{C}$.

2.1 Asymmetric ODFs Based on a Cone Model

We exemplify the idea of a cone-based directional ODF filtering by building a Gaussian function $G(\mathbf{x}, \mathbf{g_i}, \sigma)$ whose center lies on the axis of the cone with a variance parameter σ. At the voxel $\mathbf{x}$, once the cones are constructed along each sampling direction $\mathbf{g}_i$ as in Figure 1(b), the weighted smoothing of the ODFs is carried out. The corresponding Gaussian functions are also visualised in (b) which depicts the nature of the weighting going from highest on the central axis to lowest on the side surface of the cone. This filtering operation is formulated by:

$$f_{\boldsymbol{x}}(\boldsymbol{g}_i) = \sum_{\boldsymbol{v} \in \text{Cone } \boldsymbol{C}} \phi_{\boldsymbol{v}}(\boldsymbol{g}_i) G(\boldsymbol{x}, \boldsymbol{g}_i, \sigma) \ , \tag{1}$$

where $f_{\boldsymbol{x}}(\cdot)$ is the regularized ODF function at the voxel $\mathbf{x}$. Note that smoothing is performed only along the orientation of the cone $\mathbf{g_i}$, i.e., the ODF values only in the direction corresponding to that of the cone are averaged out over the voxels in the cone. Thus, via the created capability to both seeing further along a given direction in a larger neighbourhood and summing over the corresponding ODF values, the gross orientations are sharpened whereas the less important or less dominant directions are supressed. This leads to extraction of existing local asymmetries in a fiber distribution.

[1] The reconstruction of an ODF is performed by two methods: diffusion orientation transform (DOT) [12] and spherical deconvolution [13] using HARDI tools [14].

2.2 Measuring Asymmetry

Once an AODF field is constructed over the volume of interest, the asymmetry for each voxel can be computed. To this end, we formulate an index based on the angular similarity metric in Ref. [5]. Functions are envisioned to be vectors on an ∞-dimensional Hilbert space, and the cosine of the angle between two functions is a measure of their similarity. When symmetry is concerned, the functions can be taken to be the AODF denoted by $f(\hat{\boldsymbol{u}})$, and its reflection in the origin, $f(-\hat{\boldsymbol{u}})$. Thus, a similarity index is given by

$$\cos\gamma = \frac{\int_S f(\hat{\boldsymbol{u}})f(-\hat{\boldsymbol{u}})d\hat{\boldsymbol{u}}}{\int_S f(\hat{\boldsymbol{u}})^2 d\hat{\boldsymbol{u}}} = \frac{\sum_{l=0}^{l_{\max}}\sum_{m=-l}^{l}(-1)^l\,|a_{lm}|^2}{\sum_{l=0}^{l_{\max}}\sum_{m=-l}^{l}|a_{lm}|^2}\ , \tag{2}$$

where the last expression provides the measure in terms of a_{lm}, which are the coefficients obtained when $f(\hat{\boldsymbol{u}})$ is represented in a series of spherical harmonics. Then an asymmetry index α can be defined simply as

$$\alpha = \sin\gamma. \tag{3}$$

3 Experimental Results

In this section, we will show the results of cone-based directional ODF filtering and asymmetry index maps on synthetic and real data. The parameters cone height h and radius r (defined in § 2.1) are taken to be 2 voxels for synthetic experiments, they are chosen as 4 voxels for real experiments, and σ is taken to be 0.5 for all experiments; these parameters were selected heuristically.

3.1 Synthetic Bending and Crossing Fibers

In Ref. [4], diffusion taking place in a curving fiber within a full circle geometry is considered, and the signal attenuation for each portion of the curving circular fiber is derived. Using this result, we simulated the signal for a set of concentric circularly bending fibers. Then, ODFs that are based on the constructed q-space signals are reconstructed using the DOT approach [12]. One sample simulated data is shown in Figure 2. In (a), the original ODFs are depicted whereas in (b) are the resulting AODFs at each voxel corresponding to those in (a). Clearly, the proposed spatial regularisation of the ODFs resulted in an asymmetric ODF field, which is naturally in line with the underlying curving geometry where the bending structures are now visible at the voxel level. The asymmetry is visibly decreasing for larger circles as expected.

Two more synthetic examples (images are taken from the simulations in [15]) demonstrate the capabilities of the proposed technique. In Figure 3 (a,b), a half circle pattern of fibers meet a straight line of fibers in non-symmetric junctions. The ODF field shown on the left (a) displays the symmetry assumption imposed in conventional HARDI processing as seen from the visualised symmetric ODFs. However, the obtained asymmetric ODF field displayed on the right (b) reveals clearly the bending in the crossing captured at the voxel-level representations of the junction regions.

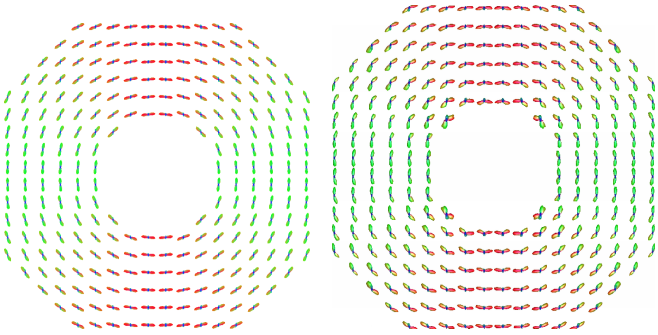

Fig. 2. Circularly bending fibers: ODF field created by the DOT method [12] (Left); asymmetric ODF field created by the proposed technique (Right).

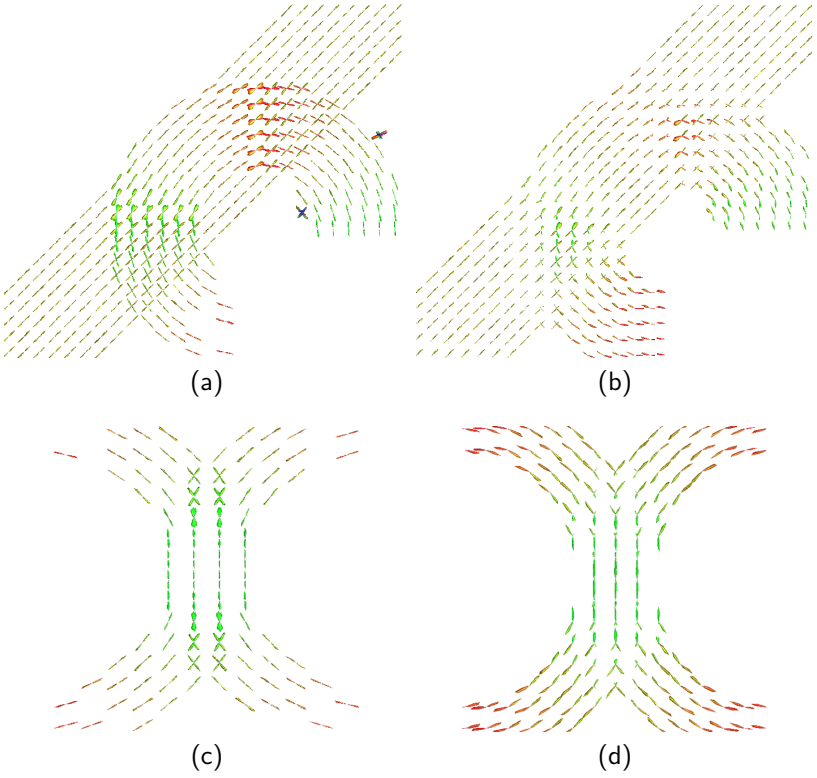

Fig. 3. Simulations for two geometries involving crossing fiber bundles. (a & c): ODFs obtained via the method in Ref. [13]. (b & d) AODF maps obtained by our technique.

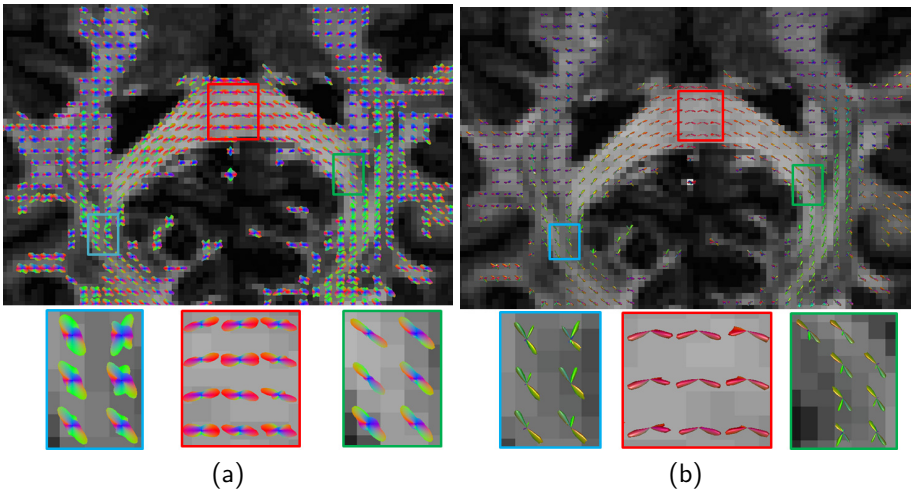

Fig. 4. An axial slice depicting the corpus callosum and Meyer's loop. ODF results obtained by the DOT method (a), and corresponding AODF maps (b) shown on fractional anisotropy maps. Three color-coded regions are magnified in the bottom rows.

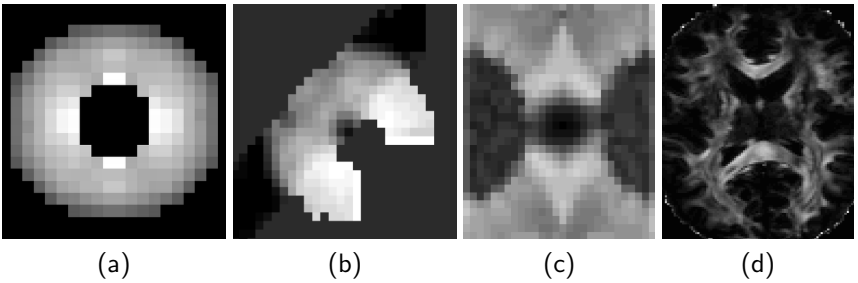

Fig. 5. Asymmetry index (α) maps (bright-to-dark:high-to-low values) calculated for: (a) circular fibers; (b) half circle crossing with a straight bundle; (c) kissing fiber configuration; (d) a slice from the HCP data.

In Figure 3 (c,d), a bottleneck or a kissing fiber geometry is depicted. On the left (c) is the ODF representation of the kissing fibers whereas on the right (d) are the corresponding reconstructed asymmetric ODFs. The resulting representation of the local fiber orientations, particularly in splaying sections of the kissing fibers are clearly observed to exhibit the Y-pattern as desired.

3.2 Results on Real Diffusion MRI Data

HARDI data was obtained from the MGH-USC Human Connectome Project (HCP) database (https://ida.loni.usc.edu/login.jsp), which is acquired from 288

gradient directions with $1.25 \times 1.25 \times 1.25\ mm^3$ voxel size. The ODF field is created by the DOT method [12]. In application of Eq. 1, we inserted a sigmoid function on the ODF to enhance very high components and suppress very low components, which are likely to be due to noise. To focus on fiber pathways that exhibit high curvature, we selected the corpus callosum (CC) and Meyer's Loop (ML) as shown in Figure 4. It is well known that non-invasive extraction of the visual pathways including CC and ML through Diffusion MRI tractography is challenging due to the strong bending, crossing and kissing geometric patterns in the relevant anatomy. The reconstructed asymmetric ODFs clearly display the inherent bending and non-symmetry at the voxel level for those white matter tracts.

3.3 Asymmetry Index Map Results

Figure 5 demonstrates the asymmetry gray scale index maps calculated over a slice of half-circle crossing straight lines, circular fibers, kissing fibers and real white matter fibers. In (a), for the circularly bending fibers, the asymmetry indices are as expected rotationally invariant and decrease from high to low radii. Similarly, the proposed index becomes larger in the asymmetric regions of interest in (b,c): the half circle itself as well as the crossing regions, and in the splaying parts of the kissing fibers, respectively. In both cases, for the fibers lying straight, the asymmetry map values are close to zero as desired. In (d), the asymmetry map for an axial slice is shown. The α values are substantial for regions with fibers featuring relatively high curvature.

4 Discussion and Conclusion

The proposed method provides an alternative representation and visualization of diffusion anisotropy that can overcome the limitations of the conventional symmetric ODF profiles, which are a product of the existing ODF reconstruction techniques. Asymmetry information is captured via an inter-voxel regularisation scheme, which produces asymmetric ODFs, indicative of the intravoxel organization. Based on the latter, an asymmetry index is also introduced.

Our experiments on both synthetic fiber populations and real MRI data demonstrated that the constructed AODFs successfully capture the intra-voxel asymmetry. We expect our method to improve tractography outcomes, where we can simply adjust conventional tractography methods such as [15] and provide faithful extraction of fiber pathways when orientational heterogeneity persists at the voxel level, particularly for fibers that exhibit intravoxel curvature, splaying, or crossings. The generated asymmetry maps were shown to accentuate strongly bending, kissing and crossing regions in fiber pathways. Such maps could be utilised to analyse white matter structures, complementing traditional measures of anisotropy and mean diffusivity in population studies and eventually improve the sensitivity and specificity of diffusion-MRI to different pathologies and processes.

References

1. Basser, P.J., Pajevic, S., Pierpaoli, C., Duda, J., Aldroubi, A.: In vivo fiber tractography using DT-MRI data. Magn. Reson. Med. 44(4), 625–632 (2000)
2. Tuch, D.S., Weisskoff, R.M., Belliveau, J.W., Wedeen, V.J.: High angular resolution diffusion imaging of the human brain. Mag. Reson. Med. 7, 321 (1999)
3. Liu, C., Bammer, R., Acar, B., Moseley, M.E.: Characterizing non-Gaussian diffusion by using generalized diffusion tensors. Magn. Reson. Med. 51(5), 924–937 (2004)
4. Özarslan, E., Koay, C.G., Basser, P.J.: Remarks on q-space MR propagator in partially restricted, axially-symmetric, and isotropic environments. Magn. Reson. Imaging 27(6), 834–844 (2009)
5. Özarslan, E., Koay, C.G., Shepherd, T.M., Komlosh, M.E., İrfanoğlu, M.O., Pierpaoli, C., Basser, P.J.: Mean apparent propagator (MAP) MRI: a novel diffusion imaging method for mapping tissue microstructure. NeuroImage 78, 16–32 (2013)
6. Ozcan, A.: Complete Fourier direct magnetic resonance imaging (CFD-MRI) for diffusion MRI. Front. Integr. Neurosci. 7, 18 (2013)
7. Anderson, A.W., Gore, J.C.: Analysis and correction of motion artifacts in diffusion weighted imaging. Magnetic Resonance in Medicine 32(3), 379–387 (1994)
8. Barmpoutis, A., Vemuri, B.C., Howland, D., Forder, J.R.: Extracting tractosemas from a displacement probability field for tractography in DW-MRI. In: Metaxas, D., Axel, L., Fichtinger, G., Székely, G. (eds.) MICCAI 2008, Part I. LNCS, vol. 5241, pp. 9–16. Springer, Heidelberg (2008)
9. Schultz, T.: Towards resolving fiber crossings with higher order tensor inpainting. In: Laidlaw, D.H., Vilanova, A. (eds.) New Developments in the Visualization and Processing of Tensor Fields, pp. 253–265 (2012)
10. Campbell, J.S.W.: Savadjiev, P., Siddiqi, K., Pike, G.: Validation and Regularization in Diffusion MRI Tractography. In: ISBI, pp. 351–354 (2006)
11. Ehricke, H.H., Otto, K.M., Klose, U.: Regularization of bending and crossing white matter fibers in MRI q-ball fields. Magn. Reson. Imaging 29, 916–926 (2011)
12. Özarslan, E., Shepherd, T.M., Vemuri, B.C., Blackband, S.J., Mareci, T.H.: Resolution of complex tissue microarchitecture using the diffusion orientation transform (DOT). NeuroImage 31(3), 1086–1103 (2006)
13. Dell'Acqua, F., Scifo, P., Rizzo, G., Catani, M., Simmons, A., Scotti, G., Fazio, F.: A modified damped Richardson-Lucy algorithm to reduce isotropic background effects in spherical deconvolution. NeuroImage 49(2), 1446–1458 (2010)
14. Canales-Rodrguez, E.J., Melie-Garca, L., Iturria-Medina, Y., Alemn-Gmez, Y.: High angular resolution diffusion imaging (HARDI) tools. `http://neuroimagen.es/webs/hardi_tools/`
15. Descoteaux, M., Deriche, R., Knsche, T.R., Anwander, A.: Deterministic and probabilistic tractography based on complex fibre orientation distributions. IEEE Trans. Med. Imaging 28(2), 269–286 (2009)